Thermo-electrical performance of PEM fuel cell using Al_2O_3 nanofluids

Irnie Zakaria [a], W.A.N.W. Mohamed [a], W.H. Azmi [b,*], A.M.I. Mamat [a], Rizalman Mamat [b,d], W.R.W. Daud [c]

[a] Faculty of Mechanical Engineering, Universiti Teknologi Mara (UiTM), 40450 Shah Alam, Selangor, Malaysia
[b] Faculty of Mechanical Engineering, Universiti Malaysia Pahang, 26600 Pekan, Pahang, Malaysia
[c] Fuel Cell Institute, Universiti Kebangsaan Malaysia, 43600 Bangi, Selangor, Malaysia
[d] Faculty of Bioengineering and Technology, Universiti Malaysia Kelantan, 17600 Jeli, Kelantan, Malaysia

ARTICLE INFO

ABSTRACT

Nanofluid adoption as an alternative coolant for Proton Exchange Membrane (PEM) fuel cell is a new embarkation which hybridizes the nanofluids and PEM fuel cell studies. In this paper, findings on the thermo-electrical performance of a liquid-cooled PEM fuel cell with the adoption of Al_2O_3 nanofluids were established. Thermo-physical properties of 0.1, 0.3 and 0.5% volume concentration of Al_2O_3 nanoparticles dispersed in water and water: Ethylene glycol (EG) mixtures of 60:40 were measured and then adopted in PEM fuel cell as cooling medium. The result shows that the cooling rate improved up to 187% with the addition of 0.5% volume concentration of Al_2O_3 nanofluids to the base fluid of water. This is due to the excellent thermal conductivity property of nanofluids as compared to the base fluid. However, there was a penalty of higher pressure drop and voltage drop experienced. Thermo electrical ratio (TER) and Advantage ratio (AR) were then established to evaluate the feasibility of Al_2O_3 nanofluid adoption in PEM fuel cells in terms of both electrical and thermo-fluid performance considering all aspects including heat transfer enhancement, fluid flow and PEM fuel cell performance. Upon analysis of these two ratios, 0.1% volume concentration of Al_2O_3 dispersed in water shows to be the most feasible nanofluid for adoption in a liquid-cooled PEM fuel cell.

© 2017 Elsevier Ltd. All rights reserved.

1. Introduction

Increase of awareness in environmental pollution and concern on fossil fuel depletion issues have diversified the search of an alternative energy source. Among the alternatives, the highlight is hydrogen as an energy carrier. Hydrogen fuel cell offers a greener solution to the conventional power conversion system as it only produces usable electricity, together with heat and water as by-products [1].

The PEM fuel cell is an electro-chemical device that utilizes hydrogen as a fuel to react with pure oxygen or surrounding air in order to generate electricity. Acceptance of hydrogen fuel cells as a viable, flexible and clean energy generator for the future has pushed the rapid progress of PEM fuel cells technology. Initiatives taken namely the use of development of better and cheaper materials with component designs that operates at greater efficiencies in order to

bring down the energy generation costs to a target of USD40/kW$_e$ [2]. Some recent trends in the advancement of PEM fuel cell technology is provided here. Less expensive carbon xerogels are replacing carbon black microporous layer as the GDL [3]. Membrane Electrode Assemblies having microporous layers with low molecular weight PDMS polymers exhibited better performance compared to PTFE and FEP based polymers [4]. Low quantities and nanosized platinum catalysts, deposited on graphene nanoplatelets, showed improved performance compared to conventional platinum loadings [5]. Membrane material has evolved from the use of Nafion® to phosphoric acid-doped PBI membranes for high temperature applications (120–200 °C) [6]. Bipolar plate designs are more diverse and applies complex geometrical gas flow fields to improve the uniformity of distribution, pressure drop and reaction at the GDL [7–10]. Highly responsive process control using advanced modeling and algorithms has been developed to optimize PEM fuel cell system hardware [11]. Meanwhile, in thermal management, effective temperature control strategies for transportation have been proposed for minimal stack temperature variation [12].

A PEM fuel cell attracts researchers especially in automotive industries due to its high energy conversion efficiency of 60% as compared to 20–30% in internal combustion engines (ICE) [13]. A

* Corresponding author.
   E-mail addresses: irnieazlin@salam.uitm.edu.my (I. Zakaria), wanajmi@salam.uitm.edu.my (W.A.N.W. Mohamed), wanazmi2010@gmail.com (W.H. Azmi), amanihsan@salam.uitm.edu.my (A.M.I. Mamat), rizalman.mamat@yahoo.com (R. Mamat), wramli@ukm.edu.my (W.R.W. Daud).

Nomenclature

A	constant in Eqs. (2) and (3)
B	constant in Eqs. (2) and (3)
C_p	specific heat, J/kg·K
AR	advantage ratio
FESEM	field emission scanning electron microscopy
EG	ethylene glycol
I	current, A
K	thermal conductivity, W/m·K
m	mass, gram
$P_{\Delta H}$	theoretical power
P_{elect}	electrical power
PEMFC	proton exchange membrane fuel cell
$\dot{Q}_c$	cooling rate
T	temperature, K
TER	thermo-electrical ratio
V	voltage, V

Greek symbols

ΔP	pressure drop
ϕ	volume concentration,%
φ	volume fraction
μ	dynamic viscosity, kg/m·s
η	efficiency
ρ	density, kg/m³
σ	electrical conductivity, μS/cm

Subscripts

bf	base fluid
eff	effective
nf	nanofluids
p	particle
r	ratio

PEM fuel cell is also favourable due to quick start up and dynamic load response [14]. Among the successful global trend setters in PEM fuel cell vehicles is Hyundai with its Tucson ix35, which is reported to have increased their production to 3600 units in early 2018 and Toyota with its Mirai that already selling more than 2800 cars through the end of 2016 [15]. Other automotive player that has ventured in PEM fuel cell vehicles is Honda with its Clarity [16].

Despite all the success stories about PEM fuel cell vehicles, there are challenges that dampen the acceleration of the technology, namely the thermal management system [17]. Small temperature differences between the ambient and operating temperatures of PEM fuel cell which is around 60–80 °C has made the heat removal far more challenging than ICE. Zhang and Kandlikar [17] estimated that the heat generated can be almost 100 kW or more for an average passenger car, which typically has a power output of more than 80 kW. The biggest portion of heat generated is dissipated through thermal management of PEM fuel cell while both reactant and product heat removal in PEM fuel cell is almost negligible. Thermal management of PEM fuel cell is vital to the stack power output performance due to the sensitivity of its membrane electrode assembly (MEA). The MEA needs to be 100% humidified for an excellent electro-chemical reaction. However, too much humidification will result in flooding issue and reduce in performance while excessive heat will put the membrane at the risk of dehydration [18].

There are various attempts done by researchers worldwide on improving thermal management but mostly it is in the active mode of heat transfer such as larger areas of radiators but it is not preferable due to the stringent packaging requirements [19]. A different approach was taken by the US Department of Energy (DoE) in passive heat transfer method which is through improving the coolant's thermo-physical property via nanofluids [20,21].

Nanofluids was initiated by Choi and Eastman [22] from Argonne National Laboratory through the dispersion of a nano sized solid particles in base fluid of water. The addition of metal particle which has significantly higher thermal conductivity as compared to base fluid has improved the heat transfer coefficient tremendously. Nanofluids superior thermo-physical properties are reported by many researchers [23–25]. Challenges in application of nanofluids in heat transfer application also highlighted by researchers especially on the stability and the high pumping power associated with nanofluids [26,27].

Nanofluids in an electrically active heat transfer application such as PEM fuel cell is relatively a new area of study thus the available literature is quite limited. In PEM fuel cell, nanofluids was previously aimed to prolong coolant's durability while preserving the low electrical conductivity of coolants even after 2 years [28]. The study also targeted to simplify liquid-cooled PEM fuel cells through the deletion of deionizers and adopting smaller water pumps through the usage of nanofluids as coolant [28]. The advantages and challenges associated with the adoption of nanofluids in PEM fuel cell has been reviewed by Zakaria et al. [29]. The obvious advantage is the superior heat transfer performance while the most challenging part is the highly conductive coolant after circulated through PEM fuel cell stack. Islam et al. [30] added another challenge which is the stability of nanofluids for PEM fuel cell. Islam et al. [31] also theoretically studied effect of the nanofluids performance to the heat exchanger and pumping power requirement of a PEM fuel cell. The study shows that there is a reduction of 21% of frontal area of heat exchanger with the adoption of 0.05 vol% of nanofluids to 50:50 (water:EG) base fluids with only 1% pumping power increment.

The strict limit of electrical conductivity requirement that needs to be maintained over time also highlighted by McMullen et al. [21] who specified that the electrical conductivity requirement is as low as 1.5 μS/cm while the fuel cell maker such as Ballard [32] outlined it to be 5 μS/cm at 20 °C as the coolant properties. This low electrical conductivity is required in order to avoid current produced by the fuel cells to leak through the conductive coolant which will eventually reduce the performance of a PEM fuel cell [33]. Thermal electrical conductivity ratio (TEC) was introduced by Zakaria et al. [34] based on the thermo-physical properties of Al_2O_3 in water and water:EG. The TEC is used to evaluate the feasibility of Al_2O_3 nanofluids adoption as coolant in PEM fuel cell. The TEC suggested that for 0.5 vol% concentration of Al_2O_3, maximum value of 50% EG content in the base fluid is still feasible for the application.

Apart from the theoretical and fundamental study on nanofluids in PEM fuel cell, performance of nanofluids in a single PEM fuel cell cooling plate has also been reviewed both experimentally and numerically by Zakaria et al. [35–37]. The study was conducted for 0.1–0.5% volume concentration of Al_2O_3 nanofluids in 50:50 (water:EG) in a single cooling plate of PEM fuel cell which was subjected to a constant heat flux of 100 W to mimic the heat generated by the PEM fuel cell. The study shows that there is an increase of 22% of heat transfer coefficient at Re 120 with 15% penalty on pumping power for 0.5 volume concentration of Al_2O_3 nanofluids as compared to conventional fluid. Zakaria et al. [38] also investigated effect of Al_2O_3 nanofluids of 0.1–0.5% volume concentration in 60:40 (water:EG) in a PEM fuel cell cooling plate and reported

that at 0.5% volume concentration of nanofluids, there is a gain of 23% higher heat transfer as compared to base fluid with 17% increase in pumping power. Meanwhile, in a full scale PEM fuel cell study, Islam et al. [39] shows that 0.5 vol% ZnO nanofluids in 50:50 (water:EG) has increased the cooling capacity by 29% as compared to conventional coolant with 10% penalty on the pumping power. This experimental study was performed on of 2.4 kW$_e$ PEM fuel cell and reported that there is a negligible effect in electrical power output of the stack with nanofluid adoption.

This study validates the previous research finding of Islam et al. [39] on the effect of high electrical conductivity property of nanofluids to the thermo-electrical performance of a PEM fuel cell. This study is also important as there is very limited experimental works reported on nanofluids in a full stack of PEM fuel cell. In this study, an actual 2.4 kW$_e$ stack of PEM fuel cell was experimented with Al$_2$O$_3$ nanofluids as the cooling medium and the thermo-electrical performance was observed. The Al$_2$O$_3$ nanofluids are selected for the study since Al$_2$O$_3$ has among the highest thermal conductivity in the oxide family of nanofluids after CuO [40]. Apart from thermal conductivity advantage, Sarojini et al. [41] has reported a lower electrical conductivity value in Al$_2$O$_3$ as compared to CuO, which is favourable to PEM fuel cell applications. Less possibility for sedimentation is also one of the factors for choosing Al$_2$O$_3$ over other nanofluids [42]. Upon completion of the study, the feasibility of the adoption is viewed from two perspectives, which are the PEM fuel cell performance perspective and thermo-fluid perspective. In the PEM fuel cell performance perspective, the cooling rate enhancement is justified over the electrical power drop as a penalty of the adoption while the thermo-fluid perspective is measured through Advantage Ratio (AR) established by Azmi et al. [43]. The AR measures the feasibility of adoption in terms of both heat transfer improvement and additional pumping power required. The finalized Al$_2$O$_3$ nanofluids at specific volume concentration in specific base fluid that fulfils both perspectives is then proposed for the adoption as an alternative coolant for a PEM fuel cell cooling.

2. Methodology

The study starts with the preparation of nanofluids and conformity on the stability of the coolant prepared. The thermo-physical characteristic measurements were then performed on the stable nanofluids before being adopted to a full scale PEM fuel cell as a cooling medium. Base line reading was first observed to verify the set up accuracy. Upon confirming the accuracy, Al$_2$O$_3$ nanofluids were then tested in the set up.

2.1. Preparation of nanofluids

The Al$_2$O$_3$ nanoparticles were procured from Sigma-Aldrich. It is 13 nm in size with 99.8% purity. The field emission scanning electron microscopy (FESEM) technique [11] was used to characterize the Al$_2$O$_3$ nanoparticles. The FESEM image under the magnification of 300,000 is shown in Fig. 1. It is observed that the Al$_2$O$_3$ nanoparticles are spherical in shape. The mixture of water and ethylene glycol of AR grade with 99.9% purity was adopted as base fluids. The two-step method was selected for the nanofluid preparation. No surfactant was used in the preparation of the nanofluids. The required mass of nanoparticles in order to obtain a specific volume concentration is calculated from Eq. (1) with reference to the density of the nanoparticle in Table 1.

$$\phi = \left(\frac{m_p}{\rho_p} \right) \Big/ \left(\frac{m_p}{\rho_p} + \frac{m_{bf}}{\rho_{bf}} \right) \times 100 \qquad (1)$$
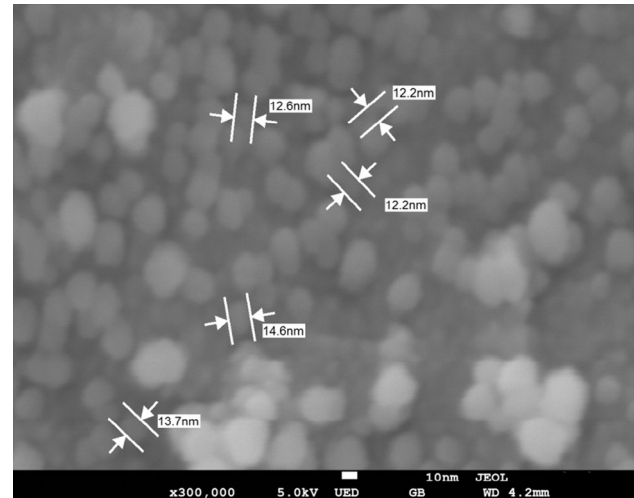

Fig. 1. Image of dry Al$_2$O$_3$ nanoparticle with FESEM at X 300,000 magnifications.

The nanofluid mixture was then homogenized via ultrasonic homogenizer for two hours to assure a stable dispersion of nanoparticles and the base fluids. The stability of the samples prepared were then analysed through both zeta potential measurement and visual observation.

2.2. Thermo-physical properties measurement

The KD2 Pro thermal property analyser of Decagon Devices, Inc., USA was used to measure the thermal conductivity of nanofluids. The same device was used in various studies of thermal conductivity [44–48]. The analyser is in compliance with the standard of ASTM D5334 and IEEE 442-1981. A water bath is used during the measurement to maintain a constant temperature of the sample with accuracy of 0.1 °C. Five measurements were taken for each volume concentration and temperature to ensure the measurements are within acceptable deviations of less than 5% from one another [47,48]. The electrical conductivity of nanofluids was measured with CyberScan PC10 which is built in with automatic temperature compensation (ATC). A 200 ml nanofluid was used for electrical conductivity measurement at room temperature of 27 °C. Sarojini et al. [41] also conducted electrical conductivity of Al$_2$O$_3$ using the same portable electrical conductivity device. The Brookfield LVDV-III Ultra Rheometer was used to measure the dynamic viscosity of nanofluids. Pak and Cho [49], Yu et al. [50] and also Namburu et al. [51] used the same instrument in their studies of nanofluid viscosity. The Rheometer is calibrated yearly to ensure the accuracy of its data. The thermo-physical property measurement devices are shown in Fig. 2.

2.3. Liquid cooled PEM fuel cell

Fig. 3 shows a liquid-cooled PEM fuel cell by Ballard FCgen 1310 used in the experiment as the fuel cell stack. The specifications of the stack are shown in Table 2 which was provided by the manufacturer. The schematic diagrams of the system are shown in Fig. 3 (a), while the actual set up is in Fig. 3(b). The complete fuel cell test bench is made up by the cooling, hydrogen and oxidant systems. The maximum stack current is 160 A, but the study was limited to 100 A due to the constraint in the current loader capacity. A constant laminar flow of Reynolds (Re) number of 1000 was used to study the effect of different nanofluids to the PEM fuel cell performance. The constant Re 1000 was achieved by having a coolant mass flow rate as tabulated in Table 3.

Table 1
Properties of nanoparticles and base fluid used in the experiment.

Nano particle/base fluid	Thermal conductivity κ, W/m·K	Electrical conductivity σ, μS/cm	Dielectic constant ε	Density ρ, kg/m^3	References
Al$_2$O$_3$	36	10^{-8}	9.1–9.3	4000	[41,49,69,70]
Distilled water	0.615	6	80	999	[41,60,69,71,72]
Ethylene glycol	0.252	1.07	38	1110	
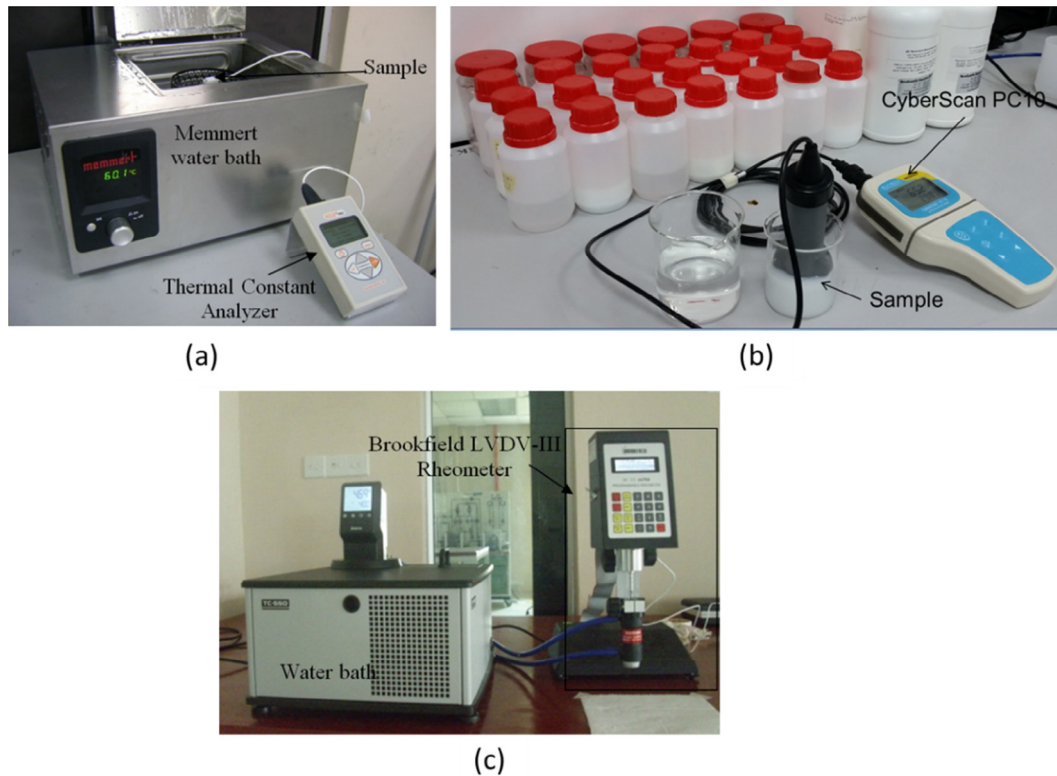
Fig. 2. Apparatus for measurement of (a) Thermal conductivity (b) Electrical conductivity (c) Dynamic viscosity.

2.4. Uncertainty analysis of PEM fuel cell set up

An uncertainty analysis of the various parameters in the experiment was determined based on uncertainty measurements of all related independent variables. The uncertainties for the main analytical parameter are estimated following the procedure given by Beckwith et al. [52]. The uncertainties of main parameters were calculated with less than 1.8%. The range of uncertainties is summarized and presented in Table 4. Detailed instrumentation error was calculated and shown in Table 5. The instrumentations were evaluated for up to 0.8% error.

3. Mathematical models

3.1. Thermo-physical properties

Sundar et al. [53] developed a thermal conductivity and viscosity model specifically tailored to Al$_2$O$_3$ in water:EG mixtures. The semi empirical correlation was also formulated based on 135 experimental data conducted for several mixtures of water:EG. It is assumed that the thermal conductivity increases linearly with particle concentration. The thermal conductivity model is given in Eq. (2).

$$\frac{K_{nf}}{K_{bf}} = A + B\phi \tag{2}$$

where;

$A = 1.1236$ and $B = 8.0175$ for 80 : 20(W : EG)nanofluids

$A = 1.0806$ and $B = 10.164$ for 60 : 40(W : EG)nanofluids

$A = 1.0618$ and $B = 10.448$ for 40 : 60(W : EG) nanofluids

The Sundar et al. [53] correlation for viscosity is shown in Eq. (3).

$$\frac{\mu_{nf}}{\mu_{bf}} = Ae^{B\phi} \tag{3}$$

where;

$A = 0.9396$ and $B = 24.16$ for 80 : 20(W : EG) nanofluids

$A = 0.9299$ and $B = 67.43$ for 60 : 40(W : EG)nanofluids

$A = 1.1216$ and $B = 77.56$ for 40 : 60(W : EG)nanofluids

The electrical conductivity model was based on the classical model of Maxwell [54] for liquid-solid suspensions, which is applicable to all homogeneous low volume fractions of nanofluids. The model predicts the effective conductivity σ$_{eff}$, as a function of the conducting nature of both particle σ$_p$, and base fluid of suspension σ$_{bf}$. The effective electrical conductivity is given by Eq. (4).
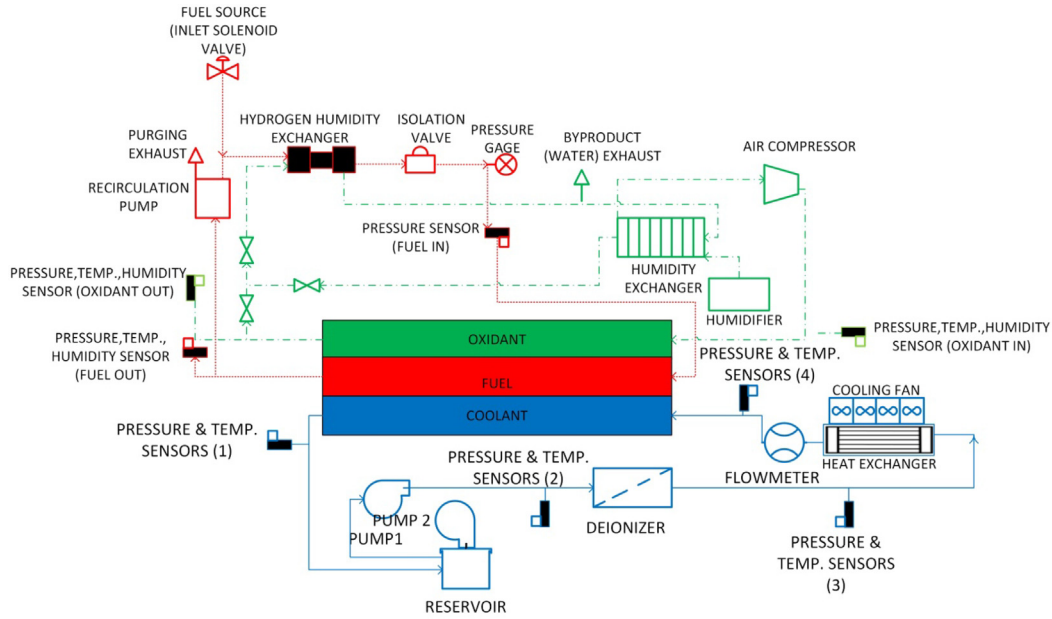
(a) The schematic diagram [68]
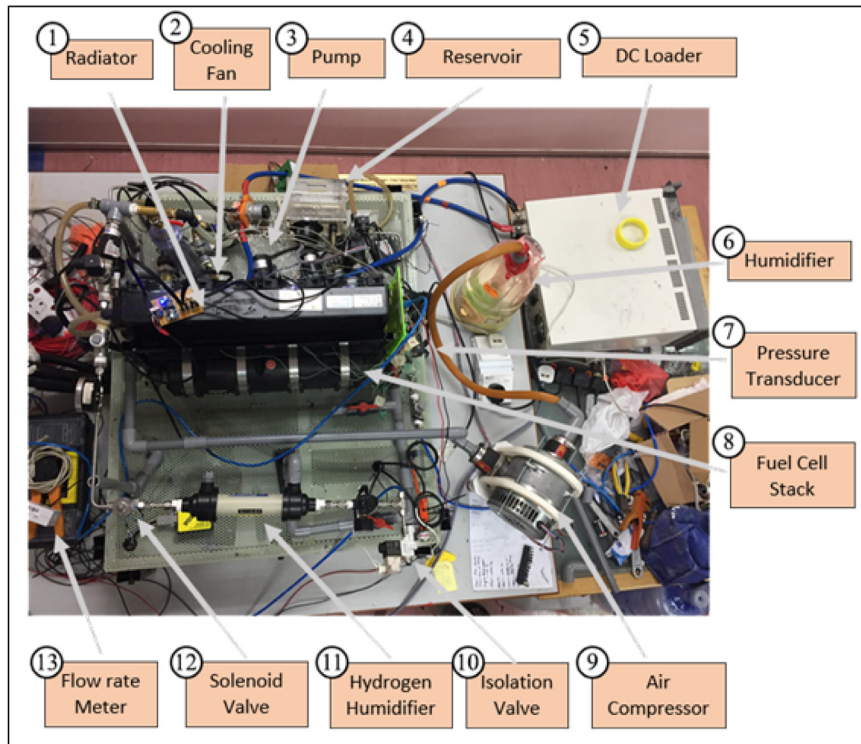
(b) Experimental set up

Fig. 3. The 2.4 kW$_e$ liquid cooled PEM fuel cell (See above-mentioned reference for further information.).

$$\sigma_{eff} = \left[1 + \frac{3(\alpha - 1)\varphi}{(\alpha + 2) - (\alpha - 1)\varphi} \right] \sigma_{bf} \tag{4}$$

where $\alpha = \frac{\sigma_p}{\sigma_{bf}}$ is the conductivity ratio of the two phases where;

(a) $\frac{\sigma_p}{\sigma_{bf}} = 1 - \frac{3}{2}\varphi$ for $\sigma_p << \sigma_{bf}$ (insulating particles)

(b) $\frac{\sigma_p}{\sigma_{bf}} = 1$, for $\sigma_p = \sigma_{bf}$ (equal conductivity)

(c) $\frac{\sigma_p}{\sigma_{bf}} = 1 + 3\varphi$, for $\sigma_p >> \sigma_{bf}$ (highly conducting particles)

3.2. PEM fuel cell thermo-electrical performance

PEM fuel cell thermo-electrical performance is characterized by the polarization curve known as an I-V curve. The potential energy input by the hydrogen, $P_{\Delta H}$ is calculated by Eq. (5).

$$P_{\Delta H} = V_{rev,cell} I \tag{5}$$

where I is the load current applied and $V_{rev,cell}$ is taken at 1.254; with the assumption that the water produced is in vapour phase [33].

The energy output, which is known as electrical power, P_{elect} produced by the cell is defined by Eq. (6).

$$P_{elect} = V_{cell}I \tag{6}$$

where V_{cell} is the experimental value.

The thermal power dissipated, $P_{thermal}$ is estimated through the thermodynamic energy balance in the cell given by Eq. (7).

$$P_{thermal} = P_{\Delta H} - P_{elect} \tag{7}$$

Conversion efficiency for a fuel cell stack is calculated using Eq. (8) [55].

$$\eta_{conv} = \frac{V_{cell}}{V_{rev,cell}} \tag{8}$$

In terms of thermo-fluid aspect, heat dissipated from the stack is absorbed by the coolant and calculated using Eq. (9) [56].

$$Q_c = mC_p\Delta T \tag{9}$$

where ΔT is referring to the difference between inlet coolant temperature and the outlet coolant temperature of the fuel cell stack.

Thermo-electrical ratio (TER) is introduced to determine the feasibility of adoption of nanofluids as an alternative coolant for PEM fuel cell. The ratio rationalizes the heat transfer enhancement in PEM fuel cell cooling rate to the penalty in performance drop of the electrical power. The TER is calculated as in Eq. (10). The higher the ratio, the more feasible the nanoparticle adoption is.

$$TER = \frac{\frac{Q_{c,nf} - Q_{c,water}}{Q_{c,water}}}{\frac{P_{elect\ water} - P_{elect\ nf}}{P_{elect\ water}}} \tag{10}$$

Advantage Ratio (AR) [43] is also calculated at this full-scale PEM fuel cell level. It is a non-dimensional parameter to determine the effectiveness of the cooling rate enhancement to the increment of the pumping power required. It is favourable to have an AR > 1 [38] for the adoption of the nanofluids in PEM fuel cell as given in Eq. (11).

$$AR_{fuel\ cell} = \frac{\frac{Q_{c,nf} - Q_{c,bf}}{Q_{c,bf}}}{\frac{\Delta P_{nf} - \Delta P_{bf}}{\Delta P_{bf}}} \tag{11}$$

4. Results and discussion

4.1. Nanofluid stability

The stability of the nanofluid samples were measured using both zeta potential and visual observation. It is observed from the high absolute value of zeta potential that there is a strong electrostatic repulsion force between particles in order to prevent attraction and collision caused by Brownian motion. A higher electrostatic repulsion will reduce the possibility of coagulation and settling of the nanofluids [57]. The Zeta potential measurement is however only available at 0.1% volume concentration due to the optical detection scheme limitation. The result for the zeta potential of 0.1% volume concentration of Al_2O_3 in 100:0 (W:EG) is 35.6, which falls in the region of stable to excellent stability [58]. The zeta potential value for 0.1% volume concentration of Al_2O_3 in

Table 2
Technical specification of PEM fuel cell stack used in the study.

Items	Specification
Rated power (kW)	2.4
DC voltage (at 135 A)	17.5
Cell count	27
Mass (with no coolant) [kg]	8.3
Fuel consumption [slpm]	26.7
Stack core dimension (Length × width × height) [mm]	233 × 490 × 180
Maximum current [A]	160
Fuel composition	Hydrogen ≥80%, nitrogen blend
Oxidant	Compressed ambient
Ambient operating temperature	−5 to 70 °C
Start-up temperature	≥−5 °C

Table 3
Summary of experimental parameter set up for the study.

No	Coolants	Coolant mass flow rate (kg/s)	Stack operating load (A)
1	100:0 (water:EG) basefluid	0.012	30–100
2	φ 0.1 Al_2O_3 in 100:0 (w:EG)	0.017	
3	φ 0.3 Al_2O_3 in 100:0 (w:EG)	0.025	
4	φ 0.5 Al_2O_3 in 100:0 (w:EG)	0.028	
5	60:40 (water:EG) basefluid	0.034	
6	φ 0.1 Al_2O_3 in 60:40 (w:EG)	0.042	
7	φ 0.3 Al_2O_3 in 60:40 (w:EG)	0.045	
8	φ 0.5 Al_2O_3 in 60:40 (w:EG)	0.053	

Table 4
Summary of uncertainty analysis.

No	Variables	Uncertainty (%)
1	Electrical power, P_{elect}	0.103–0.335
2	Coolant cooling rate, $Q_{coolant}$	0.304–0.611
3	Stack temperature, T_{stack}	1.187–1.837
4	Coolant pressure drop, ΔP	0.002–1.108

Table 5
Uncertainties of instruments and properties.

No	Instrument	Range of instrument	Variable measured	Least division in measuring instrument	Values measured in experiment		% Uncertainty	
					Min	Max	Max	Min
1	Thermocouple	0–300 °C	Coolant temperature change, $\Delta T_{coolant}$ $\Delta T_{coolant} = T_{coolant,out} - T_{coolant,in}$	$U_T = 0.1$ °C $U_{\Delta T_{coolant}} = \sqrt{0.1^2 + 0.1^2}$ $= 0.1414$	45.99	69.68	0.3075	0.2030
2	Flowmeter	0.8–8 LPM	Volume Flow rate, $\dot{V}$ Velocity, $\bar{V}$	0.01	2.469	3.364	0.405	0.297
3	Voltage	0–60 V	Voltage, V_{stack}	0.005	11.29	19.35	0.044	0.026
4	Current	0–240 A	Current, I	0.01	30.0	100.0	0.333	0.1
5	Pressure transducer	0–6895 Pa	Pressure, P	0.005	6.382	4440.299	0.784	0.001
6	Properties		Thermal conductivity, Dynamic viscosity, Electrical conductivity, Specific heat, Density				0.1	0.1

60:40 (water:EG) is 14.8. In terms of visual observation, it is also noticed that there is a minimum sedimentation in the nanofluids prepared, but only after 30 days of shelf life as illustrated in Fig. 4.

4.2. Thermo-physical properties evaluation

The thermal conductivity of Al_2O_3 nanofluids was measured at room temperature of 27 °C. It linearly increased with the increase in volume concentrations for both nanofluids as in Fig. 5(a). It is observed that Al_2O_3 in 100:0 (W:EG) increased by 1.4–8.3% as compared to the base fluids with the addition of 0.1–0.5% volume concentration of Al_2O_3 respectively. A small value of increment is also seen in thermal conductivity for Al_2O_3 in 60:40 (W:EG) with a maximum of 9.8% for 0.5% volume concentration as compared to the base fluid. The increment is due to the addition of nano-scale sized particles, which have enhanced the thermo-physical properties of nanofluids over base fluids in terms of thermal conductivity and Brownian motion [59]. However, comparatively Al_2O_3 nanofluids in 100:0 (W:EG) shows higher range of thermal conductivity value as compared to Al_2O_3 nanofluids in 60:40 (W:EG). This is due to the higher value of thermal conductivity in 100:0 (W:EG) as compared to 60:40 (W:EG) [60]. The experimental data were then validated against the semi empirical model of Sundar et al. [53] for stabilized water:EG mixtures of Al_2O_3 nanofluids and shown in Fig. 5(b). However, this model was only valid for 60:40, 40:60 and 80:20 (W:EG) mixtures. Sundar's model [53] is found to slightly overpredict the experimental values as the experimental data lies below the predicted model with a deviation range from 3 to 6%. This is probably due to the effect of the different diameter of Al_2O_3 particle used, which is 36 nm [53], while this study was conducted with Al_2O_3 particles of 13 nm diameter. Different methods and equipments used in the nanofluid preparation might also contribute to the overpredicted value.

The electrical conductivity of the base fluid is observed to significantly enhance with the addition of nanoparticles as shown in Fig. 6. The electrical conductivity of 100:0 (W:EG) with 0.5% volume concentration of Al_2O_3 nanofluids increased up to 516%. Meanwhile, the increment in electrical conductivity of Al_2O_3 nanofluids in 60:40 (w:EG) is not that significant as compared to 100:0 (W:EG). The significant enhancement of electrical conductivity in pure water is due to higher ratio of water as a polar liquid as compared to EG. Sarojini et al. [41] stated that the enhancement is due to the formation of surface charges by the effect of nanoparticle polarization once dispersed in a polar fluid. The electrical conductivity increases linearly as the volume concentration is increased. The electrical conductivity experimental data is then compared to the model of conductivity by Maxwell [54]. The model predicts that there will be a minimum increment to the electrical conductivity value due to the nature of Al_2O_3 which falls under insulating particles as simplified by Cruz et al. [61]. The Maxwell model [54] agrees with Al_2O_3 nanofluids in 60:40 (W: EG) with a deviation range from 3.5 to 17.5%. However, the model failed to predict the electrical conductivity of Al_2O_3 nanofluids in 100:0 (W:EG) base fluid as the deviation ranges from 72 to 84%. The significant increment of electrical conductivity value of Al_2O_3 nanofluids in 100:0 (W:EG) agrees well with experimental findings from Ganguly et al. [62] and Sarojini et al. [41].

The dynamic viscosity is also evaluated as it influences the operational pumping power requirement due to the additional internal friction and flow resistance to the system with the addi-
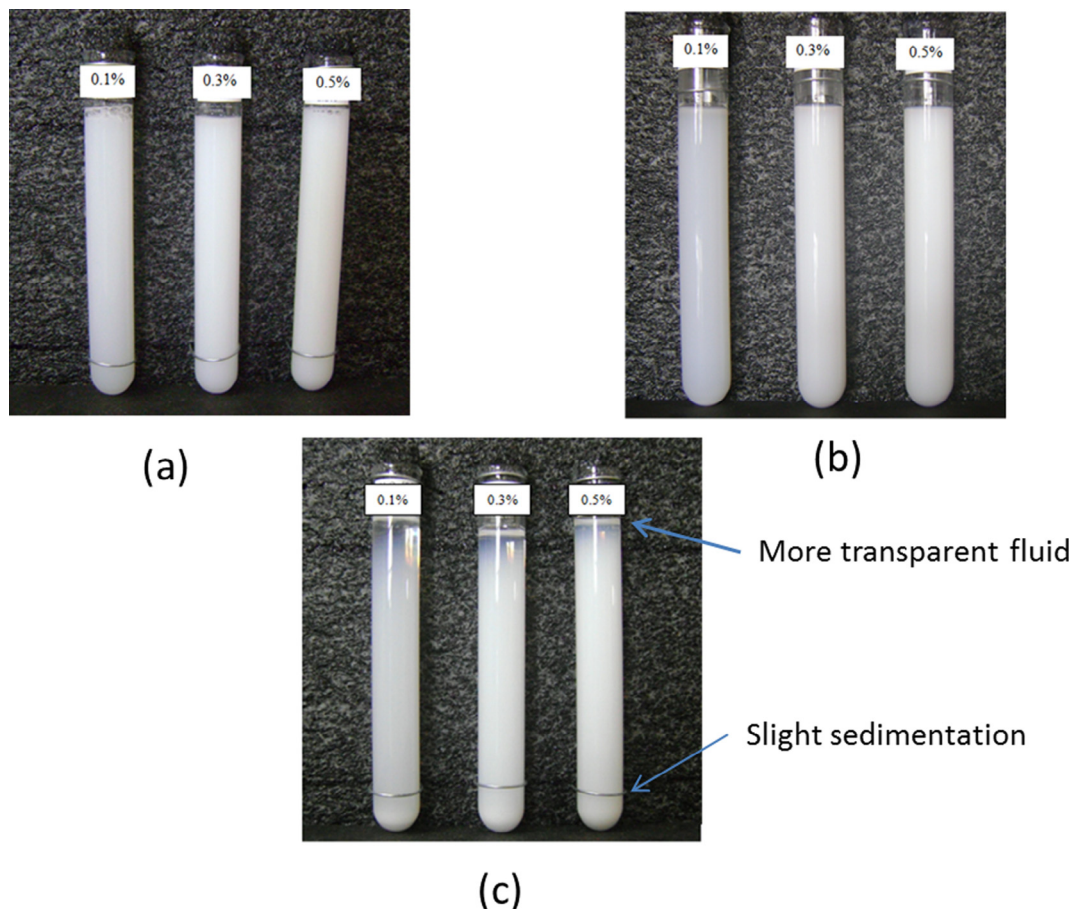

Fig. 4. Visual observation for Al_2O_3 in 100:0 (W:EG) (a) First day (b) After 30 days (c) After 10 months of preparation.
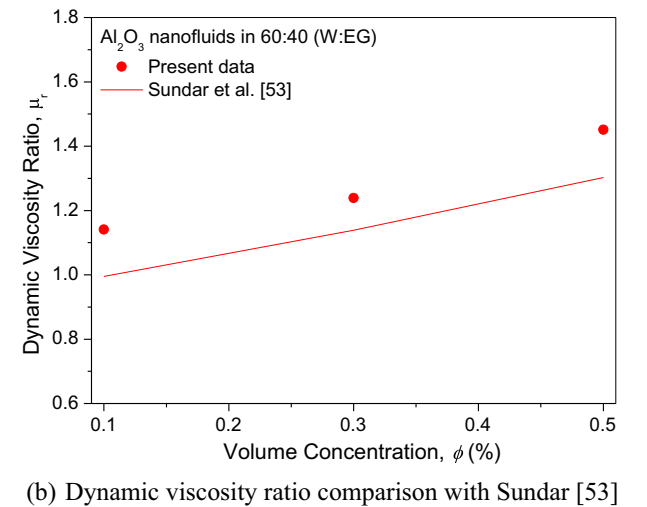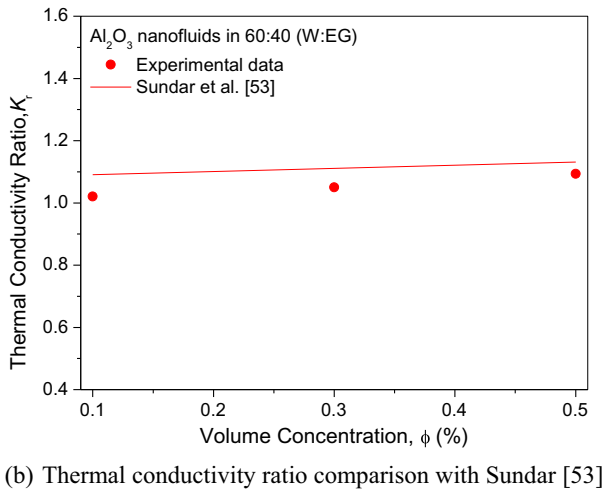
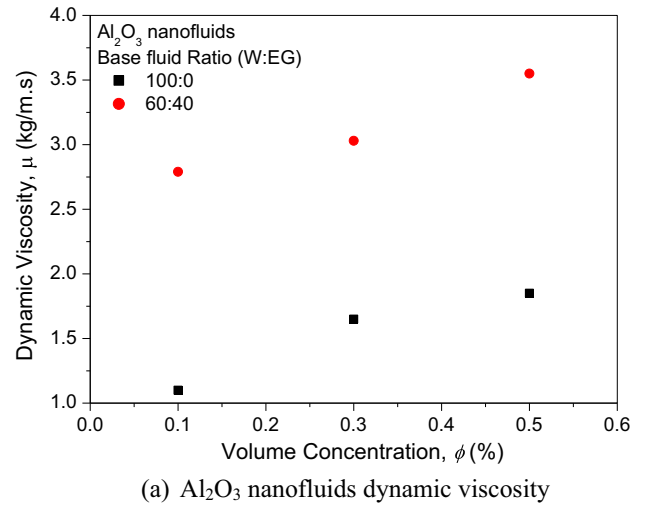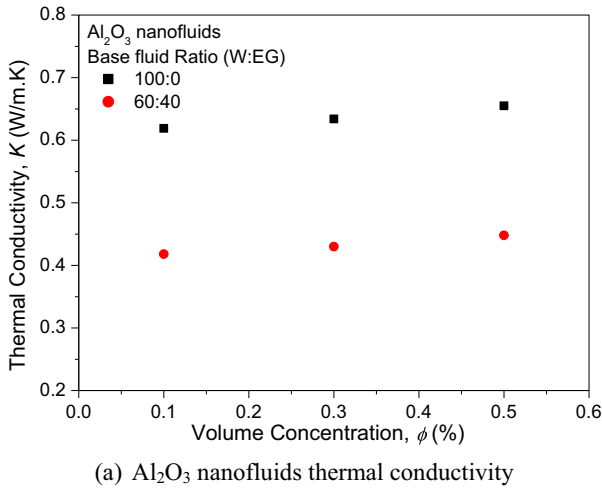(a) Al$_2$O$_3$ nanofluids thermal conductivity

(b) Thermal conductivity ratio comparison with Sundar [53]

Fig. 5. Thermal conductivity of Al$_2$O$_3$ in 100:0 (W:EG) and 60:40 (W:EG) base fluids.
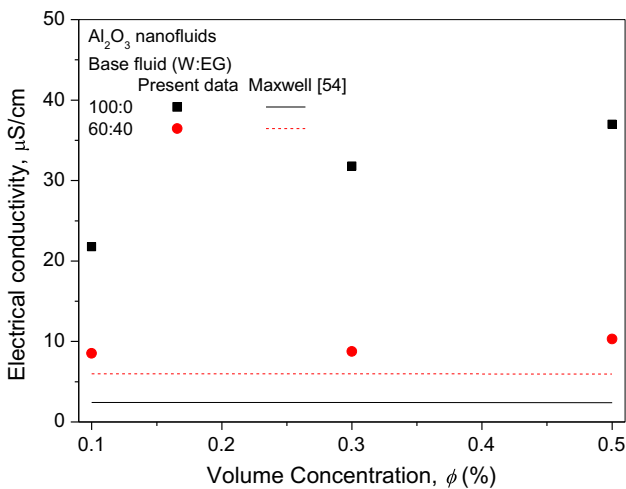

Fig. 6. Effective electrical conductivity for Al$_2$O$_3$ nanofluids and comparison against Maxwell [54].

tion of nanoparticles [40]. It is observed that the dynamic viscosity is increased with the increase in both volume concentration and EG concentration as shown in Fig. 7(a). The highest viscosity was

(a) Al$_2$O$_3$ nanofluids dynamic viscosity

(b) Dynamic viscosity ratio comparison with Sundar [53]

Fig. 7. Dynamic viscosity of Al$_2$O$_3$ in 100:0 (W:EG) and 60:40 (W:EG) base fluids.

observed at 0.5% volume concentration of nanofluids in 60:40 with 3.55 kg/m·s, while a much lower value was experienced at base fluid of 100:0 (W:EG) with 1.85 kg/m·s for the same volume concentration. This is equivalent to 45% and 116% increment in viscosity of nanofluids as compared to the base fluid of 60:40 (W:EG) and water respectively. This is contributed by the effect that the base fluid viscosity of 60:40 (W:EG) is already at a magnitude higher as compared to water thus resulting in smaller values of increment with the addition of nanoparticles [60]. Higher concentrations of nanofluids has resulted in a reduction of the natural flow around the neighbouring particles as compared to the lower ones, which in turn results in higher viscosity value [63]. The experimental dynamic viscosity values were verified against the semi-empirical model of Sundar et al. [53] as shown in Fig. 7(b). The figure shows that the experimental data is in the range of 8–14% higher than the predicted values. The under predicted model is due to the reasons explained in the thermal conductivity result previously.

4.3. PEM fuel cell thermo-electrical performance

The polarization curve or also known as an IV curve traces the changes in cell potential (voltage) due to the electrochemical reaction that consumes the reactants for electrical current generation.

In this experiment, voltage was captured in a constant coolant inlet temperature of 50 °C ± 1 °C. The IV curve for base fluid of water was initially verified against FCgen 1310 data supplied by the manufacturer [32] and it deviated in the range of 6.0–11.2% due to the effects of different balance of power plant set up used [33]. This IV curve gives indication whether any current produced by PEM fuel cell is leaking through the conductive coolant of Al_2O_3 nanofluids. The finding shows that the stack voltage is reduced with the addition of Al_2O_3 nanoparticles as compared to the base fluid. The voltage drop is most significant in the highest electrical conductivity nanofluids, which is 0.5% volume concentration of Al_2O_3 in 100:0 (W:EG), followed by 0.3% and 0.1% volume concentration as compared to base fluid of water. At 0.19 A/cm^2, the reduction of voltage is 15.6, 7.1 and 1.6% for 0.5, 0.3 and 0.1% volume concentration of Al_2O_3 as compared to base fluid of water. This finding matches the earlier results of Mohapatra et al. [64] and Maes and Lievans [65] who mentioned that fuel cell coolant has to be superior in electrical resistivity to avoid the current produced in the fuel cell to leak through the coolant. However, the voltage drop effect is not significant in Al_2O_3 nanofluid mixtures of water-EG. This is due to the small difference of the electrical conductivity value between 0.1, 0.3 and 0.5% volume concentration of Al_2O_3 in 60:40 (W:EG) as compared to the base fluid of 60:40 (W:EG). This negligible effect on the IV curve was also reported by Islam et al. [39] with the adoption of ZnO in 50:50 (W:EG) in PEM fuel cell. The effects on the IV curve of Al_2O_3 nanofluids is shown in Fig. 8.

Further investigation was done on the post experimental electrical conductivity value of Al_2O_3 nanofluids used in the experiment to validate the current leakage. The post experimental result shows that the conductive coolant does pick up free ions in the cooling line [21] as shown in Fig. 9. The electrical conductivity is higher in the post experimental reading as expected due to the current leakage from the stack to the coolant due to the lower electrical resistivity of nanofluids as compared to basefluids [33]. The 0.5% volume concentration of Al_2O_3 nanofluids in water picks up most ions from the stack as there is an addition of 29.0 μS/cm upon completion of the experiment. The electrical conductivity change is relatively lower in Al_2O_3 nanofluids in 60:40 (W:EG) as compared to Al_2O_3 nanofluids in water as the highest change is in 0.5% volume concentration with 8.6 μS/cm as compared to base fluid of 60:40 (W:EG). There are also other factors that contributes to the increase in electrical conductivity value in long term applications which include the oxidation of glycol [66] and contamination from the bipolar plate itself [67].
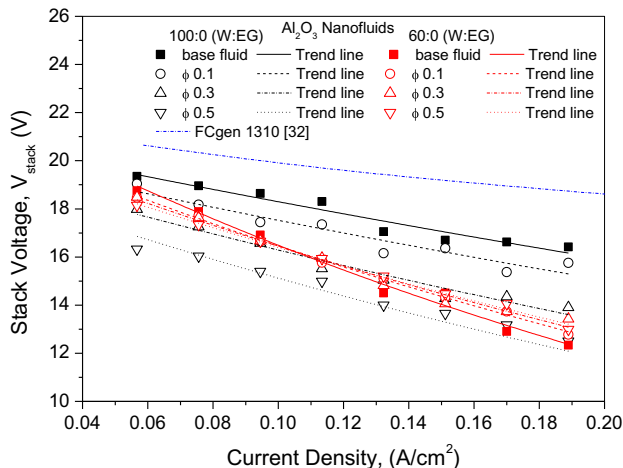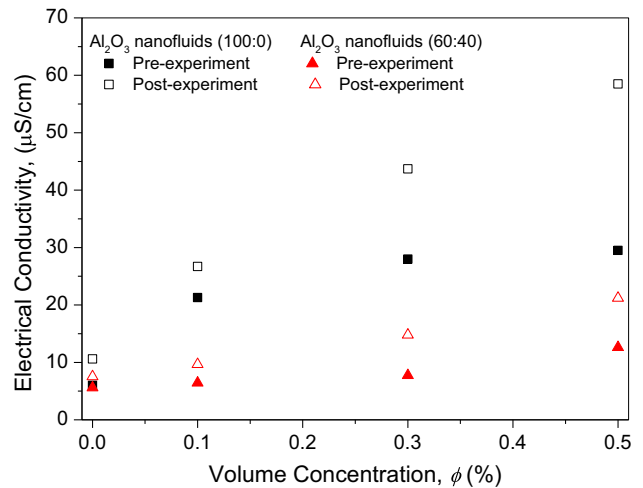

Fig. 9. Electrical conductivity values for Al_2O_3 nanofluids measured before and after experimented in PEM fuel cell.

4.4. PEM fuel cell thermo-hydraulic evaluations

The effect of cooling rates with the adoption of Al_2O_3 nanofluids is illustrated in Fig. 10. The cooling rate is exponentially increased as the current density is increased. The highest cooling rate is 0.5% volume concentration of Al_2O_3 in 100:0 (W:EG), followed by 0.5% volume concentration of Al_2O_3 in 60:40 (W:EG) and 60:40 with increment of 196.0 and 187.0% respectively as compared to base fluid of water at 0.19 A/cm^2. The hierarchy of cooling rate improvement follows the hierarchy of enhancement in thermal conductivity property of nanofluids which agrees to the expected outcome from the thermal advantage of nanofluids. Nanoparticle addition to base fluid is proven to be highly capable of increasing the convective heat transfer due to addition of surface area for heat transfer from the suspended nano-sized Al_2O_3. A higher thermal conductivity value of dispersed nanoparticles also helps to increase heat diffusion at the fluid-wall interface and across the fluid. The Brownian motion among particles also improved the heat transfer rate due to collision and interaction occurrences [30]. Base fluids of 100:0 and 60:40 (W:EG) are among the lowest cooling rate fluids as expected.

In terms of the effect to the fluid flow characteristic, the pressure difference measurement for cooling fluids at inlet and outlet

Fig. 8. Polarization curves for PEM fuel cell for Al_2O_3 nanofluids in base fluid water and 60:40 (W:EG).
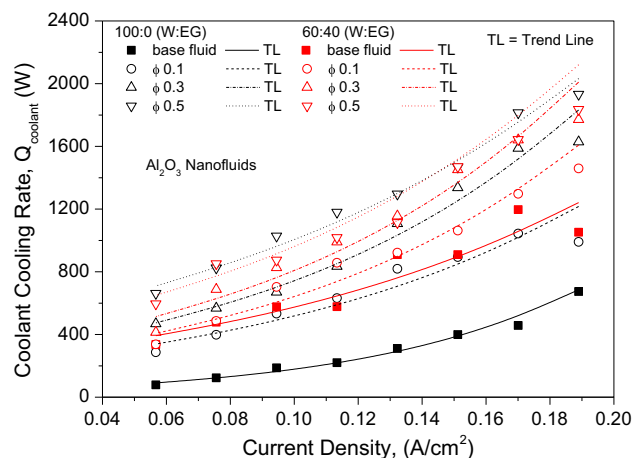

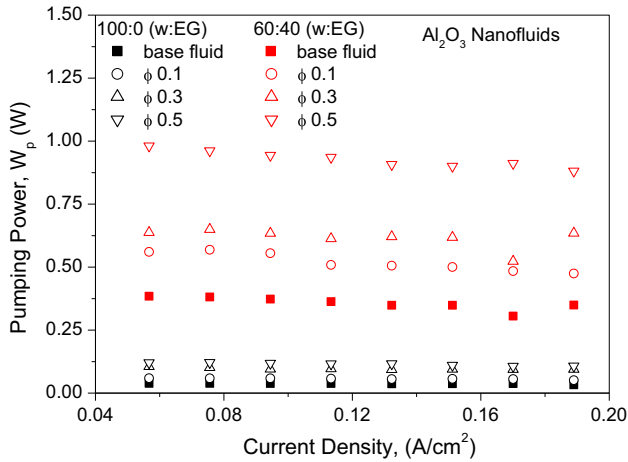Fig. 10. The cooling rate profile at increasing stack load current for base fluids and nanofluids.

Fig. 11. The pumping power requirement with the adoption of nanofluids to PEM fuel cell as cooling medium.

Fig. 12. Thermo-electrical ratio of Al_2O_3 nanofluids adoption as cooling medium in PEM fuel cell.

stack is recorded to provide the information on the additional pumping power required for Al_2O_3 nanofluids adoption in PEM fuel cell. Increase in pumping power is expected to overcome such large pressure drop across the stack due to the increase in density and viscosity properties of nanofluids as compared to base fluids. The highest pumping power was observed for 0.5% volume concentration of Al_2O_3 in 60:40 (W:EG) base fluid which is 24 times greater than water, followed by 0.3% and 0.1% volume concentration of Al_2O_3 in 60:40 (W:EG) mixture and its base fluid. The pumping power for Al_2O_3 in 100:0 (W:EG) mixtures was at a relatively lower region with the highest value given by 0.5% volume concentration of Al_2O_3 in 100:0 (W:EG), which is 2 times higher than the pumping power of water. This is then followed by 0.3%, 0.1% with base fluid of Al_2O_3 in 100:0 (W:EG) consecutively. A higher pumping power is associated with higher volume concentration as the nanoparticles provide additional internal friction and flow resistance to the system [40]. However, the pumping power increment is still acceptable due to the significant cooling rate enhancement that the Al_2O_3 nanofluids have offered. Information on the pumping power requirement is depicted in Fig. 11.

4.5. Feasibility of Al_2O_3 nanofluid adoption in PEM fuel cell

Feasibility of the adoption of Al_2O_3 nanofluids as cooling medium in PEM fuel cell is viewed from two perspectives, which are in terms of the PEM fuel cell performance and also thermo-fluid. In PEM fuel cell performance perspective, the cooling rate enhancement needs to be justified over the electrical power drop as a penalty of the adoption, termed as Thermo-electrical ratio (TER). TER is then plotted as in Fig. 12. TER is observed to drop as the current density is increased. This pattern is true to almost all of the fluids except for 0.3 and 0.5% volume concentration of Al_2O_3 in 100:0 (W:EG). These two nanofluids seem to have a linear thermo-electrical ratio with respect to current density applied. The ratio shows that 0.1% volume concentration of Al_2O_3 in 100:0 (W:EG) has the highest TER thus indicating that it is the most feasible nanofluid for PEM fuel cell in terms of PEM fuel cell performance. This is followed by 0.5% volume concentration of Al_2O_3 in 60:40 (W:EG). The next highest TER is 0.3% volume concentration of Al_2O_3 in 60:40 (W:EG), followed by 0.1% volume concentration of Al_2O_3 in 60:40 (W:EG), and base fluid in 60:40 (W:EG). The pattern showed by Al_2O_3 in 60:40 (W:EG) mixtures is consistent with the thermal conductivity value property of the fluid. However, in Al_2O_3 nanofluids of 100:0 (W:EG), the effect of high electrical conductivity value in 0.3 and 0.5% volume concentration of Al_2O_3 in 100:0
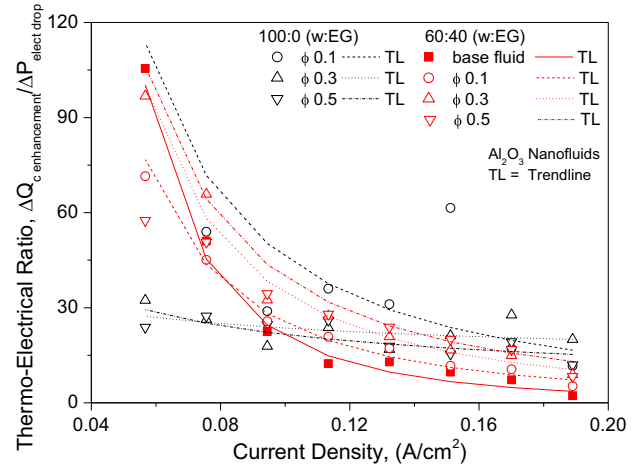
(W:EG) has resulted in a relatively large electrical power drop over the cooling rate improvement it offered thus making them the least feasible to be adopted as a PEM fuel cell cooling medium.

Another perspective considered in the adoption of Al_2O_3 nanofluids in PEM fuel cell is from its thermo-fluid point of view. The advantage ratio, AR [43] is used to determine whether the adoption of any concentration of nanofluids is beneficial from both heat transfer enhancement and fluid flow aspects. In this experiment, AR measures the cooling rate enhancement over the pressure drop penalty as shown by Fig. 13. The higher the ratio, the more advantageous the adoption of the nanofluids. The AR is also an indication of significance of cooling rate enhancement gained from the adoption of Al_2O_3 nanofluids in PEM fuel cell at the expense of pressure drop penalty. The highest region of AR is observed to be in lower Reynolds number for Al_2O_3 in 100:0 (W:EG) studied. This is due to the higher cooling rate enhancement experienced at lower current density as compared to higher current density, while the pressure drop remains consistent across the current density variation. The AR is then observed to decrease exponentially as the load is increased. The AR of Al_2O_3 nanofluids in 100:0 (W:EG) are significantly higher than the other fluids. Highest AR was given by 0.1%, followed by 0.3 and 0.5% volume concentration of Al_2O_3 nanofluids in 100:0 (W:EG). The Al_2O_3 nanofluids in 60:40 (W:EG) is observed to be in a lower region as
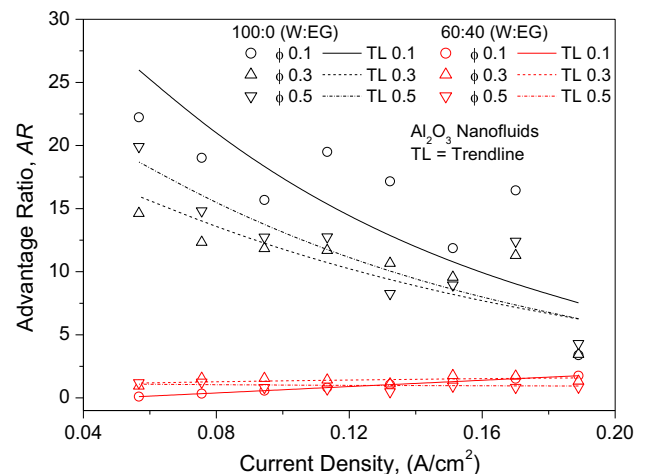

Fig. 13. Advantage ratio of base fluids and Al_2O_3 nanofluids.

compared to Al_2O_3 nanofluids in 100:0 (W:EG). The AR for Al_2O_3 nanofluids in 60:40 (W:EG) mixtures is observed to be constant with minimal effect across the current density range applied. All AR of Al_2O_3 nanofluids in 100:0 (W:EG) values are bigger than 1, which indicates that the fluids are feasible for practical adoption [43]. As for Al_2O_3 nanofluids in 60:40 (W:EG), only 0.1 and 0.3% volume concentration of Al_2O_3 in 60:40 (W:EG) barely reached the value of 1. Other than these fluids, all of them fell below 1. This indicates that Al_2O_3 nanofluids in 60:40 are less favourable as compared to Al_2O_3 nanofluids in 100:0 (W:EG). The main reason for this is due to the higher viscosity of the base fluids of 60:40 (W: EG) as compared to water [60]. Dispersion of Al_2O_3 nanoparticles in these base fluids has further increased the internal friction and lowered the AR.

5. Conclusions

In this study, potential Al_2O_3 nanofluid thermo-physical properties are measured before experimenting on a full-scale PEM fuel cell. The thermo electrical performance of PEM fuel cells and thermo-fluids characteristics of Al_2O_3 nanofluids adoption in PEM fuel cells are then presented. The Thermo Electrical ratio (TER) and the Advantage Ratio (AR) were then used to measure the feasibility of adoption. The analysis shows that 0.1% volume concentration of Al_2O_3 in 100:0 (W:EG) is the most feasible Al_2O_3 for PEM fuel cell adoption. This is justified through massive improvement in heat transfer at the expense of an acceptable electrical power drop. This was then followed by 0.3 and 0.5% volume concentration in 100:0 (W:EG). The Al_2O_3 nanofluids in 60:40 (W: EG) showed smaller TER values. The AR analysis also showed a similar pattern to TER where Al_2O_3 nanoparticles in water give the highest AR over water:EG nanofluids. It is concluded that 0.1% volume concentration of Al_2O_3 in 100:0 (W:EG) was the most feasible nanofluid for PEM fuel cell cooling medium. This has also lead to the conclusion that the adoption of EG as a base fluid to lower the electrical conductivity of coolant, therefore reducing the power loss is not a necessary countermeasure.

Conflict of interest

The authors declare that there is no conflict of interest.

Acknowledgements

Appendix A. Supplementary material

Supplementary data associated with this article can be found, in the online version, at https://doi.org/10.1016/j.ijheatmasstransfer. 2017.11.137.

References

[1] R.C. Neto, J.C. Teixeira, J.L.T. Azevedo, Thermal and electrical experimental characterisation of a 1 kW PEM fuel cell stack, Int. J. Hydrogen Energy 38 (13) (2013) 5348–5356.

[2] S. Satyapal, Hydrogen and Fuel Cells Progress Overview, in: U.S. Department of Energy Fuel Cell Technologies Office, 2017.

[3] A.M.I. Trefilov, A. Tiliakos, E.C. Serban, C. Ceaus, S.M. Iordache, S. Voinea, A. Balan, Carbon xerogel as gas diffusion layer in PEM fuel cells, Int. J. Hydrogen Energy 42 (15) (2017) 10448–10454.

[4] H. Zhang, P.K. Shen, Recent development of polymer electrolyte membranes for fuel cells, Chem. Rev. 112 (5) (2012) 2780–2832.

[5] E. Daş, S. Alkan, Gürsel, L. Isikel Sanli, A. Bayrakçeken Yurtcan, Thermodynamically controlled Pt deposition over graphene nanoplatelets: effect of Pt loading on PEM fuel cell performance, Int. J. Hydrogen Energy 42 (30) (2017) 19246–19256.

[6] S.S. Araya, F. Zhou, V. Liso, S.L. Sahlin, J.R. Vang, S. Thomas, X. Gao, C. Jeppesen, S.K. Kær, A comprehensive review of PBI-based high temperature PEM fuel cells, Int. J. Hydrogen Energy 41 (46) (2016) 21310–21344.

[7] H. Heidary, M.J. Kermani, S.G. Advani, A.K. Prasad, Experimental investigation of in-line and staggered blockages in parallel flowfield channels of PEM fuel cells, Int. J. Hydrogen Energy 41 (16) (2016) 6885–6893.

[8] T. Wilberforce, Z. El-Hassan, F.N. Khatib, A. Al Makky, J. Mooney, A. Barouaji, J. G. Carton, A.-G. Olabi, Development of Bi-polar plate design of PEM fuel cell using CFD techniques, Int. J. Hydrogen Energy 42 (40) (2017) 25663–25685.

[9] C.-J. Tseng, Y.-J. Heush, C.-J. Chiang, Y.-H. Lee, K.-R. Lee, Application of metal foams to high temperature PEM fuel cells, Int. J. Hydrogen Energy 41 (36) (2016) 16196–16204.

[10] M.Z. Chowdhury, Y.E. Akansu, Novel convergent-divergent serpentine flow fields effect on PEM fuel cell performance, Int. J. Hydrogen Energy 42 (40) (2017) 25686–25694.

[11] Y. Saygılı, S. Kıncal, I. Eroglu, Development and modeling for process control purposes in PEMs, Int. J. Hydrogen Energy 40 (24) (2015) 7886–7894.

[12] S. Cheng, C. Fang, L. Xu, J. Li, M. Ouyang, Model-based temperature regulation of a PEM fuel cell system on a city bus, Int. J. Hydrogen Energy 40 (39) (2015) 13566–13575.

[13] H. Fayaz, R. Saidur, N. Razali, F.S. Anuar, A.R. Saleman, M.R. Islam, An overview of hydrogen as a vehicle fuel, Renew. Sustain. Energy Rev. 16 (8) (2012) 5511–5528.

[14] N.L. Garland, D.C. Papageorgopoulos, J.M. Stanford, Hydrogen and fuel cell technology: progress, challenges, and future directions, Energy Procedia 28 (2012) 2–11.

[15] T.J. Times, Toyota to quadruple production of Mirai fuel-cell vehicles by 2017, 2015.

[16] J. Taylor, Honda Clarity Fuel Cell, 2017.

[17] G. Zhang, S.G. Kandlikar, A critical review of cooling techniques in proton exchange membrane fuel cell stacks, Int. J. Hydrogen Energy 37 (3) (2012) 2412–2429.

[18] K. Jiao, X. Li, Water transport in polymer electrolyte membrane fuel cells, Prog. Energy Combust. Sci. 37 (3) (2011) 221–291.

[19] R.K. Ahluwalia, X. Wang, Fuel cell systems for transportation: status and trends, J. Power Sources 177 (1) (2008) 167–176.

[20] J. Mock, P. McMullen, S. Mohapatra, Fuel Cell Coolant Optimization and scale up, Dynalene Inc, 2011.

[21] P. McMullen, S. Mohapatra, E. Donovan, Advances in pem fuel cell nano-coolant, in: Fuel Cell Seminar & Energy Exposition, Curran Associates Inc, Columbus, Ohio, USA, 2013, p. 344.

[22] S.U.S. Choi, J.A. Eastman, Enhancing Thermal Conductivity of fluids with Nanoparticles, in: ASME International Mechanical Engineering Congress & Exposition, San Francisco, CA, 1995.

[23] M.H. Hamzah, N.A.C. Sidik, T.L. Ken, R. Mamat, G. Najafi, Factors affecting the performance of hybrid nanofluids: a comprehensive review, Int. J. Heat Mass Transf. 115 (Part A) (2017) 630–646.

[24] O.A. Alawi, N.A.C. Sidik, H.W. Xian, T.H. Kean, S.N. Kazi, Thermal conductivity and viscosity models of metallic oxides nanofluids, Int. J. Heat Mass Transfer 116 (Supplement C) (2018) 1314–1325.

[25] M.N.A.W.M. Yazid, N.A.C. Sidik, W.J. Yahya, Heat and mass transfer characteristics of carbon nanotube nanofluids: a review, Renew. Sustain. Energy Rev. 80 (Supplement C) (2017) 914–941.

[26] N.A. Che Sidik, M. Mahmud Jamil, W.M.A. Aziz Japar, I. Muhammad Adamu, A review on preparation methods, stability and applications of hybrid nanofluids, Renew. Sustain. Energy Rev. 80 (Supplement C) (2017) 1112–1122.

[27] N.A.C. Sidik, M.N.A.W. Muhamad, W.M.A.A. Japar, Z.A. Rasid, An overview of passive techniques for heat transfer augmentation in microchannel heat sink, Int. Commun. Heat Mass Transfer 88 (Supplement C) (2017) 74–83.

[28] Dynalene, Dynalene FC, in: D. Inc (Ed.), 2013.

[29] I. Zakaria, Z. Michael, W.A.N.W. Mohamed, A.M.I. Mamat, W.H. Azmi, R. Mamat, R. Saidur, A review of nanofluid adoption in polymer electrolyte membrane (PEM) fuel cells as an alternative coolant, J. Mech. Eng. Sci. 8 (2015) 1351–1366.

[30] M.R. Islam, B. Shabani, G. Rosengarten, J. Andrews, The potential of using nanofluids in PEM fuel cell cooling systems: a review, Renew. Sustain. Energy Rev. 48 (2015) 523–539.

[31] M.R. Islam, B. Shabani, G. Rosengarten, Nanofluids to improve the performance of PEM fuel cell cooling systems: a theoretical approach, Appl. Energy 178 (2016) 660–671.

[32] B.P.S. Inc., FCgen®-1310 Fuel Cell Stack, in, Ballard Power Systems Inc., Canada, 2012.

[33] F. Barbir, PEM Fuel Cells: Theory and Practice, 2005.

[34] I. Zakaria, W.H. Azmi, W.A.N.W. Mohamed, R. Mamat, G. Najafi, Experimental investigation of thermal conductivity and electrical conductivity of Al_2O_3 nanofluid in water – ethylene glycol mixture for proton exchange membrane fuel cell application, Int. Commun. Heat Mass Transfer 61 (2015) 61–68.

[35] I. Zakaria, W.A.N.W. Mohamed, A.M.I.B. Mamat, R. Saidur, W.H. Azmi, R. Mamat, K.I. Sainan, H. Ismail, Thermal analysis of heat transfer enhancement and fluid flow for low concentration of Al_2O_3 water-Ethylene glycol mixture nanofluid in a single PEMFC cooling plate, Energy Procedia 79 (2015) 259–264.

[36] I. Zakaria, W.A.N.W. Mohamed, A.M.I.B. Mamat, R. Saidur, W.H. Azmi, R. Mamat, S.F.A. Talib, Experimental investigation of Al_2O_3–water Ethylene glycol

mixture nanofluid thermal behaviour in a single cooling plate for PEM fuel cell application, Energy Procedia 79 (2015) 252–258.

[37] I.A. Zakaria, W.A.N.W. Mohamed, A.M.I. Mamat, K.I. Sainan, S.F.A. Talib, Thermal performance of Al_2O_3 in water - ethylene glycol nanofluid mixture as cooling medium in mini channel, AIP Conf. Proc. 1674 (2015) 020014.

[38] I. Zakaria, W.H. Azmi, A.M.I. Mamat, R. Mamat, R. Saidur, S.F. Abu Talib, W.A.N. W. Mohamed, Thermal analysis of Al_2O_3–water ethylene glycol mixture nanofluid for single PEM fuel cell cooling plate: An experimental study, Int. J. Hydrogen Energy 41 (9) (2016) 5096–5112.

[39] R. Islam, B. Shabani, J. Andrews, G. Rosengarten, Experimental investigation of using ZnO nanofluids as coolants in a PEM fuel cell, Int. J. Hydrogen Energy 42 (30) (2017) 19272–19286.

[40] R. Saidur, K.Y. Leong, H.A. Mohammad, A review on applications and challenges of nanofluids, Renew. Sustain. Energy Rev. 15 (3) (2011) 1646–1668.

[41] K.G.K. Sarojini, S.V. Manoj, P.K. Singh, T. Pradeep, S.K. Das, Electrical conductivity of ceramic and metallic nanofluids, Colloids Surf., A 417 (2013) 39–46.

[42] S.M. Peyghambarzadeh, S.H. Hashemabadi, A.R. Chabi, M. Salimi, Performance of water based CuO and Al_2O_3 nanofluids in a Cu–Be alloy heat sink with rectangular microchannels, Energy Convers. Manage. 86 (2014) 28–38.

[43] W.H. Azmi, K.V. Sharma, P.K. Sarma, R. Mamat, S. Anuar, Comparison of convective heat transfer coefficient and friction factor of TiO_2 nanofluid flow in a tube with twisted tape inserts, Int. J. Therm. Sci. 81 (2014) 84–93.

[44] D. Wen, Y. Ding, Experimental investigation into convective heat transfer of nanofluids at the entrance region under laminar flow conditions, Int. J. Heat Mass Transf. 47 (24) (2004) 5181–5188.

[45] H.A. Mintsa, G. Roy, C.T. Nguyen, D. Doucet, New temperature dependent thermal conductivity data for water-based nanofluids, Int. J. Therm. Sci. 48 (2) (2009) 363–371.

[46] S.W. Lee, S.D. Park, S. Kang, I.C. Bang, J.H. Kim, Investigation of viscosity and thermal conductivity of SiC nanofluids for heat transfer applications, Int. J. Heat Mass Transf. 54 (1–3) (2011) 433–438.

[47] Y. He, Y. Jin, H. Chen, Y. Ding, D. Cang, H. Lu, Heat transfer and flow behaviour of aqueous suspensions of TiO_2 nanoparticles (nanofluids) flowing upward through a vertical pipe, Int. J. Heat Mass Transf. 50 (11–12) (2007) 2272–2281.

[48] Y. Ding, H. Alias, D. Wen, R.A. Williams, Heat transfer of aqueous suspensions of carbon nanotubes (CNT nanofluids), Int. J. Heat Mass Transf. 49 (1–2) (2006) 240–250.

[49] B.C. Pak, Y.I. Cho, Hydrodynamic and Heat transfer study of dispersed fluids with submicron metallic oxide particles, Exp. Heat Transfer 11 (2) (1998) 151–170.

[50] W. Yu, H. Xie, Y. Li, L. Chen, Q. Wang, Experimental investigation on the heat transfer properties of Al_2O_3 nanofluids using the mixture of ethylene glycol and water as base fluid, Powder Technol. 230 (2012) 14–19.

[51] P.K. Namburu, D.P. Kulkarni, D. Misra, D.K. Das, Viscosity of copper oxide nanoparticles dispersed in ethylene glycol and water mixture, Exp. Therm Fluid Sci. 32 (2) (2007) 397–402.

[52] T.G. Beckwith, R.D. Marangoni, J.H. Lienhard, Mechanical Measurements, Pearson Prentice Hall Upper Saddle River, NJ, 2007.

[53] L. Syam Sundar, E. Venkata Ramana, M.K. Singh, A.C.M. Sousa, Thermal conductivity and viscosity of stabilized ethylene glycol and water mixture Al_2O_3 nanofluids for heat transfer applications: an experimental study, Int. Commun. Heat Mass Transfer 56 (2014) 86–95.

[54] J.C. Maxwell, A Treatise on Electricity and Magnetism, Oxford University Press, Cambridge, U.K., 1904.

[55] J. Larminie, A. dicks, Fuel Cell Systems Explained, John Wiley and Sons Ltd., 2003.

[56] F. Incropera, D.P. Dewitt, T.L. Bergman, A.S. Lavine, Fundamental of Heat and Mass Transfer, John Wiley & Sons, 2005.

[57] D. Zhu, X. Li, N. Wang, X. Wang, J. Gao, H. Li, Dispersion behavior and thermal conductivity characteristics of Al_2O_3–H_2O nanofluids, Curr. Appl Phys. 9 (1) (2009) 131–139.

[58] J.H. Lee, K.S. Hwang, S.P. Jang, B.H. Lee, J.H. Kim, S.U.S. Choi, C.J. Choi, Effective viscosities and thermal conductivities of aqueous nanofluids containing low volume concentrations of Al_2O_3 nanoparticles, Int. J. Heat Mass Transf. 51 (11–12) (2008) 2651–2656.

[59] P. Keblinski, S.R. Phillpot, S.U.S. Choi, J.A. Eastman, Mechanisms of heat flow in suspensions of nano-sized particles (nanofluids), Int. J. Heat Mass Transf. 45 (4) (2002) 855–863.

[60] ASHRAE, 2009 ASHRAE® Handbook Fundamentals, in: Physical Properties of Secondary Coolants (Brines), 2009.

[61] R.C.D. Cruz, J. Reinshagen, R. Oberacker, A.M. Segadães, M.J. Hoffmann, Electrical conductivity and stability of concentrated aqueous alumina suspensions, J. Colloid Interface Sci. 286 (2) (2005) 579–588.

[62] S. Ganguly, S. Sikdar, S. Basu, Experimental investigation of the effective electrical conductivity of aluminum oxide nanofluids, Powder Technol. 196 (3) (2009) 326–330.

[63] H.C. Brinkman, The viscosity of concentrated suspensions and solutions, J. Chem. Phys. 20 (1952) 571–578.

[64] S. C.Mohapatra, Fuel Cell and Fuel Cell Coolant Compositions, in, US, 2006.

[65] J.-P. Maes, S. Lievens, Method for fuel cell coolant systems, in, US, 2007.

[66] G. Zhang, S.G. Kandlikar, A critical review of cooling techniques in proton exchange membrane fuel cell stacks, Int. J. Hydrogen Energy 37 (2012) 2412–2429.

[67] N.J. Dill, Fuel cell stack coolant conductivity monitoring circuit, in, US Patent 6,838,201, 2005.

[68] W.A.N.W. Mohamed, S.F.A. Talib, I.A. Zakaria, A.M.I. Mamat, W.R.W. Daud, Effect of dynamic load on the temperature profiles and cooling response time of a proton exchange membrane fuel cell, J. Energy Inst. (2017) 1–9.

[69] A.A. Minea, R.S. Luciu, Investigations on electrical conductivity of stabilized water based Al_2O_3 nanofluid, Microfluid. Nanofluid. 13 (6) (2012) 977–985.

[70] S. Aldrich, Safety Data Sheet, in: Aluminium Oxide, 2013.

[71] Y.A. Cengel, M.A. Boles, Thermodynamics – An Engineering Approach, McGraw Hill, 2007.

[72] T.M. Group, Ethylene glycol product guide, in: T.M.G.o. Companies (Ed.), The MEGlobal Group of Companies, 2008.